Electronic Transactions on Numerical Analysis.
Volume 64, pp. 109–124, 2025.

ISSN 1068–9613.
DOI: 10.1553/etna_vol64s109

ETNA
Kent State University and
Johann Radon Institute (RICAM)

SHAPE RECONSTRUCTION OF INCLUSIONS BASED ON NOISY DATA VIA MONOTONICITY METHODS FOR THE TIME-HARMONIC ELASTIC WAVE EQUATION*

SARAH EBERLE-BLICK†

Abstract. In this paper, we extend our research concerning the standard and linearized monotonicity methods for the inverse problem of the time-harmonic elastic wave equation and introduce modifications of these methods for noisy data. In more detail, the methods must provide consistent results when using noisy data in order to be able to perform simulations with real-world data, e.g., laboratory data. We therefore consider the disturbed Neumann-to-Dirichlet operator and modify the bound for the eigenvalues in the monotonicity tests for reconstructing unknown inclusions with noisy data. In doing so, we show that there exists a noise level δ_0 such that the inclusions are correctly detected and their shape is reconstructed for all noise levels $\delta < \delta_0$. Finally, we present some numerical simulations based on noisy data.

Key words. inverse problems, time-harmonic elastic wave equation, inclusion detection, noisy data, monotonicity methods

AMS subject classifications. 35R3, 74B05

1. Introduction.

Inverse elasticity problems are used in a wide variety of areas and include medical (see, e.g., [5]) and geophysical applications (described in [35]), but especially the reconstruction of inclusions in material analysis (as shown in [1] and the references therein). In this paper we focus on the shape reconstruction based on monotonicity methods for the time-harmonic wave equation developed in [17, 18] and extend these methods to noisy data, which is of great importance if we deal with data from real measurements, since there are always measurement errors to be expected.

Similar to our previous papers [17, 18], we introduce the direct problem of the time-harmonic problem as follows.

Let $\Omega \subset \mathbb{R}^3$ be an isotropic elastic body, where the properties in its linear regime are described via the Lamé parameters λ and μ. By applying time-harmonic oscillations on Ω, we are led to the Navier equation. In more detail, this equation gives the displacement field $u : \Omega \to \mathbb{R}^3$, $u \in H^1(\Omega)^3$, of the solid body Ω, due to disturbances. We specifically deal with a material body $\Omega \subset \mathbb{R}^3$ with a $C^{1,1}$ boundary and introduce the Navier equation by means of the following boundary-value problem:

$$\begin{cases} \nabla \cdot (\mathbb{C}\hat{\nabla} u) + \omega^2 \rho u = 0, & \text{in } \Omega, \\ (\mathbb{C}\hat{\nabla} u)\nu = g, & \text{on } \Gamma_N, \\ u = 0, & \text{on } \Gamma_D. \end{cases} \tag{1.1}$$

Here Γ_N and Γ_D are such that

$$\Gamma_N, \Gamma_D \subset \partial\Omega \text{ are open }, \quad \Gamma_N \neq \emptyset, \quad \partial\Omega = \overline{\Gamma}_N \cup \overline{\Gamma}_D,$$

$\hat{\nabla} u = \frac{1}{2}(\nabla u + (\nabla u)^T)$ is the symmetrization of the Jacobian or the strain tensor, and $\mathbb{C}$ is the fourth-order tensor defined by

$$(\mathbb{C}A)_{ij} = 2\mu A_{ij} + \lambda \operatorname{tr}(A)\delta_{ij}, \quad \text{where } A \in \mathbb{R}^{3\times 3},$$

*Received July 15, 2025. Accepted May 5, 2026. Published online on July 1, 2026. Recommended by Thomas Schuster.
†Mathematical Institute for Machine Learning and Data Science, Catholic University of Eichstätt-Ingolstadt, Germany (Sarah.Eberle-Blick@ku.de).

ETNA
Kent State University and
Johann Radon Institute (RICAM)

and δ_{ij} is the Kronecker delta. The Lamé parameters are specified via the scalar functions $\lambda, \mu \in L^\infty_+(\Omega)$, which determine the elastic properties of the material, $\rho \in L^\infty_+(\Omega)$ is the density of the material, $\omega \neq 0$ is the angular frequency of the oscillation, and ν is the outward-pointing unit normal vector to the boundary $\partial\Omega$. The vector field $g \in L^2(\Gamma_N)^3$ can be understood as the source of the oscillation, and since, by Hooke's law, $\mathbb{C}\hat{\nabla}u$ equals the Cauchy stress tensor, we see that the boundary condition g specifies the traction on the surface $\partial\Omega$. We assume that $\omega \in \mathbb{R}$ is not a resonance frequency, which is a common assumption, since then the problem (1.1) has a unique solution for a given boundary condition $g \in L^2(\Gamma_N)^3$.

Finally, we give a more descriptive formulation of the forward problem (1.1). An exemplary setting of the problem of time-harmonic elasticity is given in Figure 1.1.

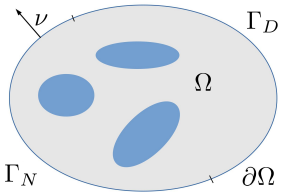

FIG. 1.1. *Exemplary setting of the problem of time-harmonic elasticity: test object Ω with its corresponding boundary $\partial\Omega$ and unknown inclusions (blue).*

The input parameters for the *direct problem* are the tractions on the Neumann boundary Γ_N, given fixed material parameters λ, μ, and ρ, and the Dirichlet condition mounts the test object in space. The solution in space of this problem yields the displacement on Γ_N.

In contrast, the input parameters for the *inverse problem* are the measured displacements on the boundary Γ_N resulting from the application of tractions. Based on this, the aim is to detect the shape of the unknown inclusions, knowing only the measurements on the boundary.

The idea for the detection of inclusions in an object by means of monotonicity tests is to apply a boundary load on different patches of its surface and to examine the resulting displacement using the Neumann-to-Dirichlet operator. In order to detect inclusions, the displacement is now simulated successively under the same traction for the homogeneous test object except for a known smaller test inclusion (made of a different material). By comparing the simulated displacements with the measured displacement in the body with the complete inclusion, it can now be detected whether a test block lies within the inclusion of the model to be tested or not.

We will solve the inverse problem by means of monotonicity methods and define the Neumann-to-Dirichlet map $\Lambda : L^2(\Gamma_N)^3 \to L^2(\Gamma_N)^3$ as

$$\Lambda : g \mapsto u|_{\Gamma_N}. \tag{1.2}$$

Thus, Λ maps the traction to the displacement $u|_{\Gamma_N}$ on the Neumann boundary.

Our aim is to formulate the standard and linearized monotonicity tests for noisy data. This problem can be handled by modifying the bound for the eigenvalues in the monotonicity tests to obtain the same reconstruction as without noise, as long as the noise does not exceed the maximal noise level δ_0. Please note that the maximal noise level depends on the number of boundary loads used, as shown in [15] for the static case.

We remark that monotonicity methods do not differentiate between different types of noise, as long as the stochastic or deterministic error does not exceed the maximal noise level δ_0. From an engineering point of view, we will deal with measurement errors.

ETNA
Kent State University and
Johann Radon Institute (RICAM)

As can be seen later in Figures 5.3 and 5.7, noiseless reconstruction results in the correct detection of the inclusions. Both monotonicity methods can handle small amounts of noise, with the standard monotonicity method being more robust regarding noise than the linearized method. By contrast, the standard method is much slower. These results are similar to those for the stationary case; see [11].

Before we extend the monotonicity methods from [17, 18] to noisy data, we give a short overview of the methods applied so far. Most of the methods are iterative (see, e.g., [4, 7, 20]) and based on regularization techniques for minimization problems, but there are also non-iterative methods such as linear sampling methods and factorization methods. In more detail, [31] develop a continuation method with respect to the frequency for the inverse problem in two dimensions to reconstruct inclusions. The reconstruction of constitutive parameters in isotropic linear elasticity from noisy full-field measurements (measurements inside the whole domain under consideration) using a regularization technique can be found in [3]. In [2], an error-in-constitutive-equation (ECE) approach to derive the Lamé parameters for time-harmonic elasticity is examined. The method is based on the minimization of an energy-based cost functional. The authors of [20] recover piecewise-constant Lamé parameters for an unknown fixed-density model. They provide a Lipschitz stability result for the inverse problem as well as a multi-level inversion scheme. A reconstruction of the boundary of a scatterer in a homogeneous medium from far-field data is considered in [30, 32]. To this end, they develop a sampling method in 2D, whereas [28] propose a factorization method in two and three dimensions (2D and 3D). In [19, 26, 27] a factorization method is described as well. Here, the focus lies on the inverse elastic scattering problem from periodic rigid structures in 2D. In [10] inverse elastic scattering problems are considered by means of the factorization method, too. In addition, the monotonicity method was adapted to the elasto-oscillatory inverse problem by the author in [17, 18].

For the 3D case, uniqueness theorems for the direct and inverse obstacle scattering problems are introduced in [21]. A uniqueness theorem in inverse scattering of elastic waves based on the far field is shown in [6] for piecewise-constant density and constant Lamé parameters. A further uniqueness result can be found in [29], where only μ is considered, i.e., $\lambda = 0$. In addition, the background shear modulus μ_0 and $\rho = \rho_0$ are assumed to be constant. A Lipschitz-type stability estimate assuming that the density is piecewise-constant is shown in [9] for constant Lamé parameters and in [8] for piecewise-constant Lamé parameters. Further on, we mention the work [17], where the localized potentials were analyzed and their existence was proven by the Runge approximation.

The basic idea of the monotonicity method was first worked out and numerically tested in [33, 34]. In addition, the monotonicity methods have already been successfully implemented in theory and practice for electrical impedance tomography (see, e.g., [22, 25]), the Helmholtz equation (see [23, 24]) as well as stationary (see [11, 12, 15] and for Lipschitz stability [13]) and time-harmonic elasticity; see [17, 18]. Here we would particularly like to highlight the possible application in the field of materials science, as already demonstrated in stationary laboratory experiments to detect aluminum inclusions in a macrolon plate; see [14]. Further on, we mention the work [16], which is concerned with Bayesian experimental design for linear elasticity.

In this paper we focus on the examination of the monotonicity methods for noisy data and the corresponding numerical simulations, which are required if we deal, for example, with real-world data of a laboratory experiment; see [14] for the stationary case.

The paper is organized as follows. We have started with the introduction of the inverse problem as well as an overview of the methods applied so far for solving this problem. In Section 2, we state the required definitions, and we summarize the results concerning the

ETNA
Kent State University and
Johann Radon Institute (RICAM)

standard and linearized monotonicity methods in Section 3. After that, we come to the main part of this paper, where we extend the monotonicity methods to noisy data and prove the resulting monotonicity tests. Finally, we present several numerical examples based on noisy data.

2. Definitions and other preliminaries. In order to provide the corresponding background, we summarize the required definitions and preliminaries. We remark that the notation is to a large extent the same notation as in [17]. The following definitions related to function spaces are used throughout the paper.

The space $H^k(\Omega)$ denotes the $L^2(\Omega)$-based Sobolev space with k weak derivatives. In addition, we define

$$L^\infty_+(\Omega) := \{f \in L^\infty(\Omega) : \operatorname{essinf}_\Omega f > 0\}.$$

We use the notation Z^n for a function space Z with $Z^n := Z \times \cdots \times Z$, where the right-hand side contains n copies of Z. We define the L^2-inner product by $(\cdot,\cdot)_{L^2}$, so that

$$(u,v)_{L^2(\Omega)^{n\times m}} := \int_\Omega u : v \,\mathrm{d}x, \quad u,v \in L^2(\Omega)^{n\times m}, \quad n,m \geq 1,$$

where : is the Frobenius inner product defined below. For orthogonality with respect to the inner product $(\cdot,\cdot)_{L^2}$, we apply the notation $\perp$, unless otherwise stated, so that

$$u \perp v \quad \Longleftrightarrow \quad (u,v)_{L^2(\Omega)^n} = 0, \quad \text{when } u,v \in L^2(\Omega)^n.$$

For the well-posedness of problem (1.1), the bilinear form B related to equation (1.1) is considered, which is given by

$$B(u,v) := -\int_\Omega 2\mu\hat{\nabla}u : \hat{\nabla}v + \lambda\nabla\cdot u\nabla\cdot v - \omega^2\rho u\cdot v \,\mathrm{d}x,$$

for all $u,v \in H^1(\Omega)^3$. The Frobenius inner product $A : B$ is defined as

$$A : B = \sum A_{ij}B_{ij}, \quad A,B \in \mathbb{R}^{m\times n}.$$

Note that the Euclidean norm on $\mathbb{R}^{m\times n}$, $m,n \in \mathbb{N}$, is given by $|A| = (A : A)^{1/2}$, for $A \in \mathbb{R}^{m\times n}$. We further introduce the notation

$$L_{\lambda,\mu,\rho}u := \nabla\cdot(\mathbb{C}\hat{\nabla}u) + \omega^2\rho u.$$

We remark that in an isotropic medium characterized by the Lamé parameters, the above equation simplifies to

$$L_{\lambda,\mu,\rho}u = \nabla\cdot(2\mu\hat{\nabla}u + \lambda(\nabla\cdot u)I) + \omega^2\rho u.$$

A weak solution to (1.1) is defined as $u \in H^1(\Omega)^3$, for which $u|_{\Gamma_D} = 0$ and

$$B(u,v) = -\int_{\Gamma_N} g\cdot v \,\mathrm{d}S, \quad \forall\, v \in \{u \in H^1(\Omega)^3 \,:\, u|_{\Gamma_D} = 0\}.$$

For the existence and uniqueness of a weak solution to (1.1), when ω is not a resonance frequency; see [17, Corollary 3.4].

The existence and uniqueness of a weak solution to (1.1) implies that the Neumann-to-Dirichlet (NtD) map Λ given by (1.2) is well defined. The map Λ is related to B as follows.

ETNA
Kent State University and
Johann Radon Institute (RICAM)

When the material parameters are regular, and u solves (1.1) with g, and v solves (1.1) with h, we see by integrating by parts that

$$B(u,v) = -\int_{\Gamma_N} g \cdot v \, \mathrm{d}S = -(g, \Lambda h)_{L^2(\Gamma_N)^3}.$$

We abbreviate the boundary condition in (1.1) by

$$\gamma_{\mathbb{C},\Gamma} u = (\mathbb{C}\hat{\nabla} u)\nu|_\Gamma,$$

or with $\gamma_{\mathbb{C}} u$ if the boundary is clear from the context. Note that all these pieces of notation are formal when $u \in H^1(\Omega)^3$, since we cannot in general take the trace of an $L^2(\Omega)^3$ function. In the low-regularity case we understand the boundary condition in a weak sense. We define $\gamma_{\mathbb{C}} u \in L^2(\Gamma_N)^3$, with $u \in H^1(\Omega)^3$ that solves (1.1), as the element in $L^2(\Gamma_N)^3$, for which

$$-(\gamma_{\mathbb{C}} u, \varphi|_{\Gamma_N})_{L^2(\Gamma_N)^3} = B(u,\varphi), \quad \forall\, \varphi \in H^1(\Omega)^3.$$

Next we give a definition of the notion of the outer support of a function or a set. The outer support (with respect to $\partial\Omega$) of a measurable function $f : \Omega \to \mathbb{R}$ is defined as

$$\operatorname{osupp}(f) := \Omega \setminus \bigcup \{U \subset \Omega : U \text{ is relatively open and connected to } \partial\Omega, f|_U \equiv 0\}.$$

For more on this see [25]. It will be convenient to extend this definition to sets. We define the outer support of a measurable set $D \subset \Omega$ (with respect to $\partial\Omega$) as

$$\operatorname{osupp}(D) := \operatorname{osupp}(\chi_D),$$

where χ_D is the characteristic function of the set D.

3. Summary of the monotonicity methods. We give a short summary of the two monotonicity methods we consider. We will take a look at the standard (see Section 3.1) as well as the linearized (see Section 3.2) monotonicity method with which we can reconstruct the set $\operatorname{osupp}(D)$, where

$$D = \operatorname{supp}(\lambda - \lambda_0) \cup \operatorname{supp}(\mu - \mu_0) \cup \operatorname{supp}(\rho - \rho_0),$$

as we did in [17, 18]. We introduce the mixed eigenvalue problem from [17] and state the corresponding proposition.

PROPOSITION 3.1 (see Proposition 3.3 from [17]). *There exists a sequence of eigenvalues $\sigma_k \in \mathbb{R}$ such that*

$$\sigma_1 \geq \sigma_2 \geq \sigma_3 \geq \cdots \to -\infty$$

and such that the mixed eigenvalue problem

$$\begin{cases} \nabla \cdot (\mathbb{C}\hat{\nabla}\varphi_k) + \omega^2 \rho \varphi_k = \sigma_k \varphi_k, \\ \gamma_{\mathbb{C}} \varphi_k|_{\Gamma_N} = 0, \\ \varphi_k|_{\Gamma_D} = 0, \end{cases} \tag{3.1}$$

has a non-zero solution $\varphi_k \in H^1(\Omega)^3$. We have moreover that:

1. *the eigenvalues $\{\sigma_k\}$ are of finite multiplicity and the eigenfunctions $\{\varphi_k\}$ form an orthonormal basis in $L^2(\Omega)^3$; and*
2. *there are only finitely many positive eigenvalues $\{\sigma_1, \ldots, \sigma_K\}$.*

ETNA
Kent State University and
Johann Radon Institute (RICAM)

We define the quantity $d(\lambda, \mu, \rho)$ as

$$d(\lambda, \mu, \rho) := \text{the number of positive elements in the sequence } \{\sigma_k\} \text{ of eigenvalues of (3.1)} \tag{3.2}$$

We will consider inhomogeneities in the material parameters of the following type. Let $D_1, D_2, D_3 \Subset \Omega$. We now assume that $\lambda, \mu, \rho \in L^\infty_+(\Omega)$ are such that

$$\begin{aligned} \lambda(x) &= \lambda_0 + \chi_{D_1}(x)\psi_\lambda(x), \quad \psi_\lambda \in L^\infty(\Omega), \quad \psi_\lambda(x) > n_1, \\ \mu(x) &= \mu_0 + \chi_{D_2}(x)\psi_\mu(x), \quad \psi_\mu \in L^\infty(\Omega), \quad \psi_\mu(x) > n_2, \\ \rho(x) &= \rho_0 - \chi_{D_3}(x)\psi_\rho(x), \quad \psi_\rho \in L^\infty(\Omega), \quad n_3 < \psi_\rho(x) < N_3, \end{aligned} \tag{3.3}$$

where the constants $\lambda_0, \mu_0, \rho_0 > 0$, the bounds $n_1, n_2, n_3 > 0$, and $\rho_0 > N_3$. The coefficients λ, μ, and ρ model inhomogeneities in an otherwise homogeneous background medium given by the coefficients λ_0, μ_0, and ρ_0.

Next we define the test coefficients $\lambda^\flat$, $\mu^\flat$, and $\rho^\flat$. Let $B \subset \Omega$ be an open set. We let

$$\begin{aligned} \lambda^\flat(x) &= \lambda_0 + \alpha_1\chi_B(x), \\ \mu^\flat(x) &= \mu_0 + \alpha_2\chi_B(x), \\ \rho^\flat(x) &= \rho_0 - \alpha_3\chi_B(x), \end{aligned} \tag{3.4}$$

where $\alpha_j > 0$ are constants and χ_B is the characteristic function with respect to the test inclusion B.

3.1. Standard monotonicity test. The following theorem gives the background for the standard monotonicity tests for exact data.

THEOREM 3.2 (see Theorem 6.4 from [17]). *Let $D := D_1 \cup D_2 \cup D_3$, where the sets are as in (3.3), and $B \subset \Omega$ and $\alpha_j > 0$ be as in (3.4), and set $\alpha := (\alpha_1, \alpha_2, \alpha_3)$. Let $M_s \in \mathbb{R}$ be defined as*

$$M_s := d(\lambda_0, \mu_0, \rho_0),$$

where $d(\lambda_0, \mu_0, \rho_0)$ is the number of positive eigenvalues of $L_{\lambda_0,\mu_0,\rho_0}$ as defined in (3.2).

The following hold:

1. *Assume that $B \subset D_j$, for $j \in J$, for some $J \subset \{1, 2, 3\}$. Then for all α_j with $\alpha_j \leq n_j$, $j \in J$, and $\alpha_j = 0$, $j \notin J$, the map $\Lambda^\flat - \Lambda$ has at most M_s negative eigenvalues.*
2. *If $B \not\subset \operatorname{osupp}(D)$, then for all α, $|\alpha| \neq 0$, the map $\Lambda^\flat - \Lambda$ has more than M_s negative eigenvalues.*

Here Λ is the Neumann-to-Dirichlet map for the coefficients in (3.3) and $\Lambda^\flat$ is the Neumann-to-Dirichlet map for the coefficients in (3.4), and the eigenvalues of $\Lambda^\flat - \Lambda$ are counted with multiplicity.

3.2. Linearized monotonicity test. Next, we present the main theorem underlying our linearized monotonicity tests. In the following, let u_g and u_f be the solutions of the boundary-value problem (1.1) for given boundary loads g and f, respectively. We introduce the associated bilinear form of the Fréchet derivative $\Lambda'_{\lambda,\mu,\rho}$ as in [18]:

$$\left(\Lambda'_{\lambda,\mu,\rho}[\hat\lambda, \hat\mu, \hat\rho]g, f\right)_{L^2(\Gamma_N)^3} = -\int_\Omega 2\hat\mu\hat\nabla u_g : \hat\nabla u_f + \hat\lambda\nabla\cdot u_g \nabla\cdot u_f - \omega^2\hat\rho u_g \cdot u_f \,\mathrm{d}x.$$

ETNA
Kent State University and
Johann Radon Institute (RICAM)

THEOREM 3.3 (see Theorem 6.1 from [18]). *Let $D := D_1 \cup D_2 \cup D_3$, where the sets are as in (3.3), and $B \subset \Omega$ and $\alpha_j > 0$, and set $\alpha := (\alpha_1, \alpha_2, \alpha_3)$. Let*

$$\mathcal{M} := \#\{\sigma \in \operatorname{Spec}(\Lambda_0 + \Lambda_0'[\alpha_1, \alpha_2, -\alpha_3] - \Lambda) : \sigma < 0\},$$

where Λ_0 and Λ are the NtD maps for the coefficients λ_0, μ_0, ρ_0 and λ, μ, ρ, respectively, and where $\Lambda_0'[\alpha_1, \alpha_2, -\alpha_3] := \Lambda_0'[\alpha_1\chi_B, \alpha_2\chi_B, -\alpha_3\chi_B]$. There exists a $\gamma_0 > 0$ such that the following hold:

1. *Assume that $B \subset D_j$, for $j \in J$, for some $J \subset \{1, 2, 3\}$. Then for all α_j with $\alpha_j \leq \gamma_0$, $j \in J$, and $\alpha_j = 0$, $j \notin J$, we have that $\mathcal{M} < \infty$.*
2. *If $B \not\subset \operatorname{osupp}(D)$, then for all α, $|\alpha| \neq 0$, we have $\mathcal{M} = \infty$.*

LEMMA 3.4. *Let the assumptions of Theorem 3.3 hold. Let*

$$\mathcal{M}_k := \#\{\sigma \in \operatorname{Spec}(\Lambda_0 + \Lambda_0'[\alpha_1\chi_{B_k}, \alpha_2\chi_{B_k}, -\alpha_3\chi_{B_k}] - \Lambda) : \sigma < 0\},$$

where Λ_0 and Λ are the NtD maps for the coefficients λ_0, μ_0, ρ_0 and λ, μ, ρ, respectively. Further, let $\mathcal{B} = \{B_k \mid B_k \subset \Omega\}$ be a fixed finite set. Then there exist a $\gamma_0 > 0$ and an $M_l \geq 0$ such that the following hold:

1. *Assume that $B_k \subset D_j$, for $j \in J$, for some $J \subset \{1, 2, 3\}$. Then for all α_j with $\alpha_j \leq \gamma_0$, $j \in J$, and $\alpha_j = 0$, $j \notin J$, we have that $\mathcal{M}_k \leq M_l$.*
2. *If $B_k \not\subset \operatorname{osupp}(D)$, then for all α, $|\alpha| \neq 0$, we have $\mathcal{M}_k > M_l$.*

Proof. Assume that $B_k \subset D_j$, for $j \in J$, for some $J \subset \{1, 2, 3\}$. Then for all α_j with $\alpha_j \leq \gamma_0$, $j \in J$, and $\alpha_j = 0$, $j \notin J$, we have that $\mathcal{M}_k$ is finite due to Theorem 3.3. Hence, we set

$$M_l = \max_{\{k \mid \mathcal{M}_k < \infty\}} \mathcal{M}_k.$$

Then $M_l < \infty$, since the set $\mathcal{B}$ is finite as well. Furthermore, $\mathcal{M}_k \leq M_l$ due to the construction of M_l.

On the other hand, if $B_k \not\subset \operatorname{osupp}(D)$, then, for all α, $|\alpha| \neq 0$, we have $\infty = \mathcal{M}_k > M_l$ due to Theorem 3.3. ∎

4. Monotonicity tests for noisy data. Next, we formulate the monotonicity tests for noisy data and prove the corresponding theorems.

4.1. Standard monotonicity test. We start with the standard monotonicity tests for noisy data.

THEOREM 4.1. *Let $D := D_1 \cup D_2 \cup D_3$, where the sets are as in (3.3), $B \subset \Omega$, and $\alpha_j > 0$ be as in (3.4), and set $\alpha := (\alpha_1, \alpha_2, \alpha_3)$. Let $M_s \in \mathbb{R}$ be defined as*

$$M_s := d(\lambda_0, \mu_0, \rho_0),$$

where $d(\lambda_0, \mu_0, \rho_0)$ is the number of positive eigenvalues of $L_{\lambda_0, \mu_0, \rho_0}$ as defined in (3.2). Further, let

$$\|\Lambda^\delta(\lambda, \mu, \rho) - \Lambda(\lambda, \mu, \rho)\| < \delta.$$

Then there exists a maximal noise level $\delta_0 > 0$ such that, for all $0 < \delta < \delta_0$, we have the following statements:

1. *Assume that $B \subset D_j$ for $j \in J$, for some $J \subset \{1, 2, 3\}$. Then, for all α_j with $\alpha_j \leq n_j$, $j \in J$, and $\alpha_j = 0$, $j \notin J$, the map $\Lambda^\flat - \Lambda^\delta$ has at most M_s eigenvalues smaller than $-\delta$.*

ETNA
Kent State University and
Johann Radon Institute (RICAM)

2. *If $B \not\subset \operatorname{osupp}(D)$, then, for all α, $|\alpha| \neq 0$, the map $\Lambda^\flat - \Lambda^\delta$ has more than M_s eigenvalues smaller than $-\delta$.*

Here Λ^δ is the Neumann-to-Dirichlet map for the noisy problem.

Proof. We start with the case $B \not\subset D$. Then $\Lambda^\flat - \Lambda$ is compact and self-adjoint and by [17, Theorem 6.5] there exists a finite-dimensional subspace V of $L^2(\Gamma_N)^3$ and a $g \in V^\perp$ with

$$((\Lambda^\flat - \Lambda)g, g) \not\geq 0$$

with $\dim(V) = M_s$. Hence, $\Lambda^\flat - \Lambda$ has more than M_s negative eigenvalues. Let $\theta < 0$ be the smallest negative eigenvalue with corresponding eigenvector $g \in V^\perp$. Then

$$\begin{aligned}((\Lambda^\flat - \Lambda^\delta)g, g) &\leq ((\Lambda^\flat - \Lambda)g, g) + \delta\|g\|^2 \\ &= (\theta + \delta)\|g\|^2 \\ &< -\delta\|g\|^2\end{aligned}$$

for all $0 < \delta < \delta_0 := -\theta/2$.

On the other hand, if $B \subset D$, then, for all $g \in V^\perp$,

$$((\Lambda^\flat - \Lambda^\delta)g, g) \geq -\delta\|g\|^2. \qquad \square$$

All in all, we end up with the following algorithm for the reconstruction based on noisy data with the standard monotonicity test.

Algorithm 1 Reconstruction of the inclusion $\operatorname{osupp}(D) \subset \Omega$.

1: Choose a set $\mathcal{B} = \{B \subset \Omega\}$ and set $\mathcal{A} = \{\}$.
2: Choose $\tilde{M}_s$.
3: **for** $B \in \mathcal{B}$ **do**
4: **for** $\Lambda^\flat$ with varied parameters by Theorem 4.1 **do**
5: Compute $\mathcal{M}_B := \sum_{\sigma_k < -\delta} 1$, where σ_k are the eigenvalues of $\Lambda^\flat - \Lambda^\delta$
6: **if** $\mathcal{M}_B \leq \tilde{M}_s$ **then**
7: Add B to the approximating collection $\mathcal{A}$, since Theorem 4.1 suggests
8: that $B \subset \operatorname{osupp}(D)$.
9: **else**
10: Discard B, since $B \not\subset D_j$, $j = 1, 2, 3$.
11: **end if**
12: **end for**
13: **end for**
14: Compute the union of all elements in $\mathcal{A}$ and all components of $\Omega \setminus \bigcup \mathcal{A}$ not connected to $\partial\Omega$. The resulting set is an approximation of $\operatorname{osupp}(D)$.

4.2. Linearized monotonicity test. We continue with the linearized monotonicity tests.

THEOREM 4.2. *Let $D := D_1 \cup D_2 \cup D_3$, where the sets are as in (3.3), and let $\mathcal{B} = \{B_k \mid B_k \subset \Omega\}$ be fixed and finite. Further, let $\alpha_j > 0$, and set $\alpha := (\alpha_1, \alpha_2, \alpha_3)$. Let*

$$\mathcal{M}_k := \#\{\sigma \in \operatorname{Spec}(\Lambda_0 + \Lambda_0'[\alpha_1\chi_{B_k}, \alpha_2\chi_{B_k}, -\alpha_3\chi_{B_k}] - \Lambda^\delta) : \sigma < -\delta\},$$

where Λ_0 and Λ are the NtD maps for the coefficients λ_0, μ_0, ρ_0 and λ, μ, ρ, respectively, so that

$$\|\Lambda^\delta(\lambda, \mu, \rho) - \Lambda(\lambda, \mu, \rho)\| < \delta.$$

ETNA
Kent State University and
Johann Radon Institute (RICAM)

Then there exists a $\gamma_0 > 0$, an $M_l \geq 0$, and a maximal noise level $\delta_0 > 0$ such that, for all $0 < \delta < \delta_0$, we have the following statements:

1. *Assume that $B_k \subset D_j$, for $j \in J$, for some $J \subset \{1,2,3\}$. Then for all α_j with $\alpha_j \leq \gamma_0$, $j \in J$, and $\alpha_j = 0$, $j \notin J$, we have that $\mathcal{M}_k \leq M_l$.*
2. *If $B_k \not\subset \operatorname{osupp}(D)$, then for all α, $|\alpha| \neq 0$, we have $\mathcal{M}_k > M_l$.*

Proof. We start with the case $B_k \not\subset D$. For this, $\Lambda_0 + \Lambda_0'[\alpha_1\chi_{B_k}, \alpha_2\chi_{B_k}, -\alpha_3\chi_{B_k}] - \Lambda$ is compact and self-adjoint, and by [18, Theorem 6.1] as well as Lemma 3.4, there exists a finite-dimensional vector space V of dimension M_l and a $g \in V^\perp$ with

$$((\Lambda_0 + \Lambda_0'[\alpha_1\chi_{B_k}, \alpha_2\chi_{B_k}, -\alpha_3\chi_{B_k}] - \Lambda)g, g) \not\geq 0.$$

Hence, $\Lambda_0 + \Lambda_0'[\alpha_1\chi_{B_k}, \alpha_2\chi_{B_k}, -\alpha_3\chi_{B_k}] - \Lambda$ has more than M_l negative eigenvalues. Let $\theta < 0$ be the smallest negative eigenvalue with corresponding eigenvector $g \in V^\perp$. Then

$$\begin{aligned}
&((\Lambda_0 + \Lambda_0'[\alpha_1\chi_{B_k}, \alpha_2\chi_{B_k}, -\alpha_3\chi_{B_k}] - \Lambda^\delta)g, g) \\
&\quad \leq ((\Lambda_0 + \Lambda_0'[\alpha_1\chi_{B_k}, \alpha_2\chi_{B_k}, -\alpha_3\chi_{B_k}] - \Lambda)g, g) + \delta\|g\|^2 \\
&\quad = (\theta + \delta)\|g\|^2 \\
&\quad < -\delta\|g\|^2
\end{aligned}$$

for all $0 < \delta < \delta_0 := -\theta/2$.

On the other hand, if $B_k \subset D$, then via Lemma 3.4, we have that for all $g \in V^\perp$

$$((\Lambda_0 + \Lambda_0'[\alpha_1\chi_{B_k}, \alpha_2\chi_{B_k}, -\alpha_3\chi_{B_k}] - \Lambda^\delta)g, g) \geq -\delta\|g\|^2. \qquad \square$$

In order to close this section, we formulate the corresponding algorithm.

Algorithm 2 Linearized reconstruction of $\operatorname{osupp}(D) \subset \Omega$.

Choose a set $\mathcal{B} = \{B \subset \Omega\}$ and set $\mathcal{A} = \{\}$.
Choose $\tilde{M}_l$.
for $B \in \mathcal{B}$ **do**
  for $\Lambda^\flat$ with parameters varied as suggested by Theorem 4.2 **do**
    Compute $\mathcal{M}_B := \sum_{\sigma_k < -\delta} 1$, where σ_k are the eigenvalues of
    $\Lambda_0 + \Lambda_0'[\alpha_1, \alpha_2, -\alpha_3] - \Lambda^\delta$
    if $\mathcal{M}_B < \tilde{M}_l$ **then**
      Add B to the approximating collection $\mathcal{A}$, since Theorem 4.2 suggests
      that $B \subset \operatorname{osupp}(D)$.
    else
      Discard B, since by Theorem 4.2 $B \not\subset D_j$, $j = 1,2,3$.
    end if
  end for
end for
Compute the union of all elements in $\mathcal{A}$ and all components of $\Omega \setminus \bigcup \mathcal{A}$ not connected to $\partial\Omega$. The resulting set is an approximation of $\operatorname{osupp}(D)$.

ETNA
Kent State University and
Johann Radon Institute (RICAM)

5. Numerical simulations. We introduce the noise matrix as

$$E = \frac{\tilde{E}}{\|\tilde{E}\|},$$

where $\tilde{E}$ is uniformly random on $[-1, 1]$ and define the perturbed Neumann-to-Dirichlet operator via

$$\Lambda^\delta = \Lambda + \eta\|\Lambda\|E.$$

It holds that

$$\|\Lambda - \Lambda^\delta\| < \delta.$$

Indeed, we have

$$\|\Lambda^\delta - \Lambda\| = \left\|(\Lambda + \eta\|\Lambda\|E - \Lambda)\right\| = \underbrace{\eta\|\Lambda\|}_{=\delta}.$$

This means for our monotonicity methods that in the standard tests

$$\Lambda^\flat - \Lambda^\delta$$

has at most M_s eigenvalues smaller than $-\delta$ and in the linearized test

$$\Lambda_0 + \Lambda_0'[\alpha_1, \alpha_2, -\alpha_3] - \Lambda^\delta$$

has at most M_l eigenvalues smaller than $-\delta$, if the test inclusion B is part of the inclusion to be reconstructed.

Based on Algorithms 1 and 2, we present some numerical tests and examine an artificial test object with two inclusions (blue) shown in Figure 5.1. The size of our test object is $1\,\mathrm{m}^3$.

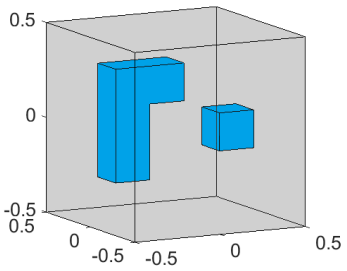

FIG. 5.1. *Cube with two inclusions (blue) (similar to the model in [11]).*

The parameters of the corresponding materials are given in Table 5.1

TABLE 5.1
Lamé parameter λ and μ in $[Pa]$ and density ρ in $[kg/m^3]$.

Material	λ_i	μ_i	ρ_i
$i = 0$: background	$6 \cdot 10^5$	$6 \cdot 10^3$	$3 \cdot 10^3$
$i = 1$: inclusion	$2 \cdot 10^6$	$2 \cdot 10^4$	$1 \cdot 10^3$

ETNA
Kent State University and
Johann Radon Institute (RICAM)

Given an angular frequency ω, the s-wavelength and p-wavelength for the homogeneous background material are defined via

$$l_p = 2\pi \frac{v_p}{k} \quad \text{and} \quad l_s = 2\pi \frac{v_s}{k}$$

with the velocities

$$v_p = \sqrt{\frac{\lambda_0 + 2\mu_0}{\rho_0}} \quad \text{and} \quad v_s = \sqrt{\frac{\mu_0}{\rho_0}}.$$

Furthermore, we deal with different numbers of test inclusions. The test inclusions consist of same-size cubes distributed on a $5 \times 5 \times 5$ or $10 \times 10 \times 10$ lattice, resulting in 125 or 1000 test cubes. We start with 125 test cubes as shown in Figure 5.2.

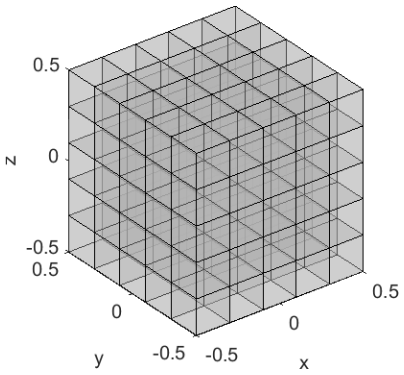

FIG. 5.2. *Dimensions and location in 3D space of the 125 test cubes.*

REMARK 5.1. We remark that the test inclusions are not aligned with the reconstruction grid and do not fill the whole inclusion, since they are slightly smaller. In order to avoid any "inverse crime", we further use different meshes for computing solutions for the forward problem as well as the reconstruction.

5.1. Standard monotonicity test. We start with the standard monotonicity tests and consider different noise levels η for the frequency $\omega = 50$ rad/s; see Figures 5.3–5.5. In this example, we assume that the bottom of the test object is fixed and each of the remaining five surfaces is divided into 10×10 patches, where we apply a normal force on each patch successively which results in 500 boundary loads.

Summarizing the results concerning the standard tests, we observe that we can reconstruct the inclusions for the prescribed noise levels η with the chosen values of δ as given in the captions of Figures 5.3–5.5.

Finally, we examine the relation of $\tilde{M}_s$, δ, and the noise level η. As can be seen in the eigenvalue plots of Figures 5.3–5.5, there exists a distinct gap between the eigenvalues of blocks inside and outside of the inclusion for a noise level $\eta = \delta = 0$.

ETNA
Kent State University and
Johann Radon Institute (RICAM)

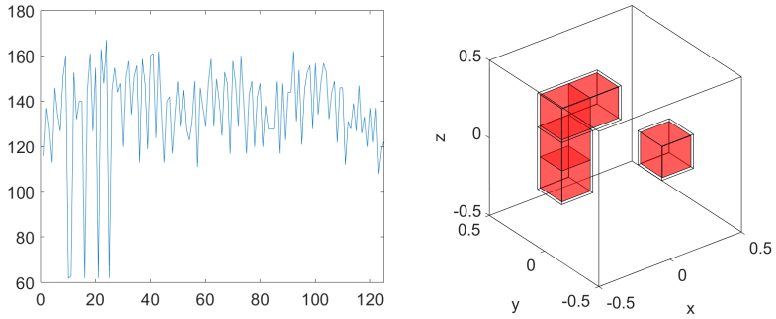

FIG. 5.3. *Left: Plot of the number of negative eigenvalues (y-axis) with block index on the x-axis. Right: Shape reconstruction in 3D space for* $\omega = 50\,rad/s$ *(*$l_p = 1.79\,m$*,* $l_s = 0.18\,m$ *for the homogeneous background material) for noise level* $\eta = 0$ *and* $\tilde{M}_s = 107$.

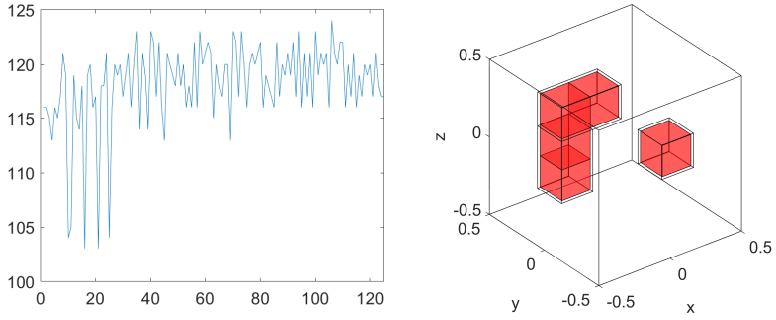

FIG. 5.4. *Left: Plot of the number of negative eigenvalues (y-axis) with block index on the x-axis. Right: Shape reconstruction in 3D space for* $\omega = 50\,rad/s$ *(*$l_p = 1.79\,m$*,* $l_s = 0.18\,m$ *for the homogeneous background material) for noise level* $\eta = 0.005$*,* $\delta = 1 \cdot 10^{-6}$*, and* $\tilde{M}_s = 107$.

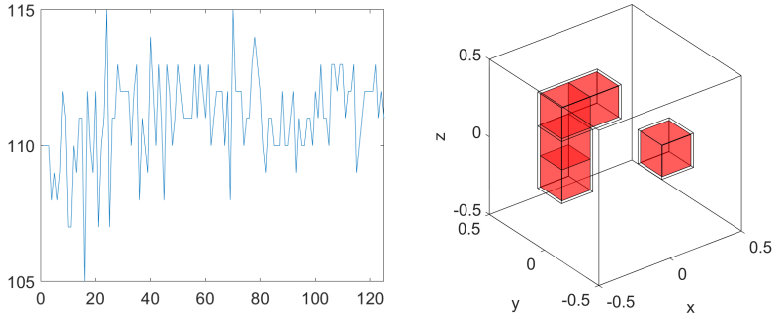

FIG. 5.5. *Left: Plot of the number of negative eigenvalues (y-axis) with block index on the x-axis. Right: Shape reconstruction in 3D space for* $\omega = 50\,rad/s$ *(*$l_p = 1.79\,m$*,* $l_s = 0.18\,m$ *for the homogeneous background material) for noise level* $\eta = 0.025$*,* $\delta = 4.54 \cdot 10^{-6}$*, and* $\tilde{M}_s = 107$.

ETNA
Kent State University and
Johann Radon Institute (RICAM)

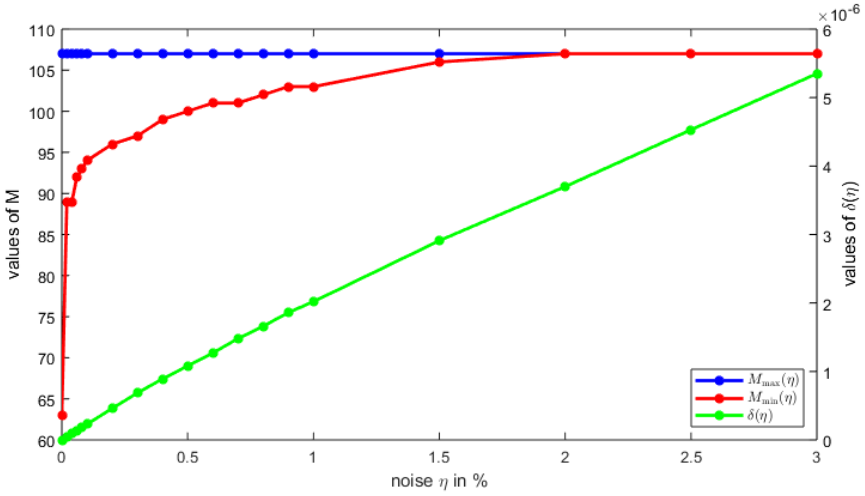

FIG. 5.6. *Plot of the relation of the bounds $M_{\min}$ and $M_{\max}$ and δ for different noise levels η.*

It is advantageous for the reconstruction to choose a large $\tilde{M}_s$ for the number of negative eigenvalues which still guarantees a correct reconstruction in the noiseless case. This is denoted by $\tilde{M}_s = M_{\max}$ in Figure 5.6. Still, a correct reconstruction at noise level η and the corresponding $\delta(\eta)$ is possible for all $M_{\min} \leq \tilde{M}_s \leq M_{\max}$. With increased noise, this gap closes fast, while the δ to be selected grows almost linearly in our test example up to a noise level of $\eta = 3\%$. Here, a reconstruction is still possible, since $M_{\min}(\eta) = M_{\max}(\eta)$. For higher noise levels, a correct reconstruction is no longer possible. Hence, a fixed $\tilde{M}_s = 107$ independent of η leads to a correct reconstruction for all noise levels satisfying the conditions of Theorem 4.1 or 4.2.

5.2. Linearized monotonicity test. Next, we take a look at the reconstructions based on the linearized monotonicity tests and consider the noise levels $\eta = 0$ (see Figure 5.7) and $\eta = 0.004$ (see Figure 5.8) for the frequency $\omega = 50$ rad/s.

Comparing the results of the standard monotonicity methods as shown in Figure 5.4 ($\eta = 0.005$) as well as Figure 5.5 ($\eta = 0.025$) with the result of the linearized monotonicity method in Figure 5.8 ($\eta = 0.004$), we see that the standard tests are more robust with respect to noise. However, a reconstruction is still possible. The main advantage of the linearized tests is the extremely reduced computation time.

Thus, we present a further test model, where we increase the number of boundary loads to include tangential components (1500 boundary loads) and also increase the resolution by using 1000 pixels compared to the 125 in the previous figures. The Dirichlet boundary and the Neumann patches remain as before. A comparable calculation for the standard monotonicity tests is not feasible due to the computation time.

It should be noted that a correct reconstruction of the inclusion is not possible even in the noiseless case, as can be seen in Figure 5.9. This is not surprising since those results were already observed in the stationary and oscillatory case in [11, 17]. However, a reconstruction for a comparable noise level as used in Figure 5.10 still separates the calculated inclusions as well as the general shape and size. It is expected to further increase the resolution by either taking more boundary loads into account (which increases the computation time) or performing the reconstruction based on the simultaneous use of a finite set of distinct frequencies, which will be the subject of further research.

ETNA
Kent State University and
Johann Radon Institute (RICAM)

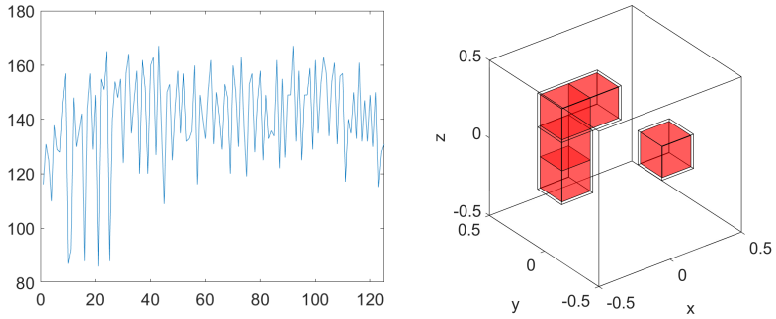

FIG. 5.7. *Left: Plot of the number of negative eigenvalues (y-axis) with block index on the x-axis. Right: Shape reconstruction in 3D space for* $\omega = 50\,rad/s$ *(*$l_p = 1.79\,m$*,* $l_s = 0.18\,m$ *for the homogeneous background material) for noise level* $\eta = 0$ *and* $\tilde{M}_l = 108$*.*

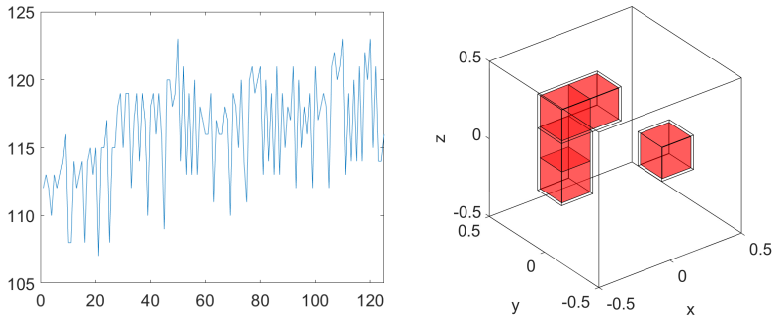

FIG. 5.8. *Left: Plot of the number of negative eigenvalues (y-axis) with block index on the x-axis. Right: Shape reconstruction in 3D space for* $\omega = 50\,rad/s$ *(*$l_p = 1.79\,m$*,* $l_s = 0.18\,m$ *for the homogeneous background material) for noise level* $\eta = 0.004$*,* $\delta = 1.92 \cdot 10^{-6}$*, and* $\tilde{M}_l = 108$*.*

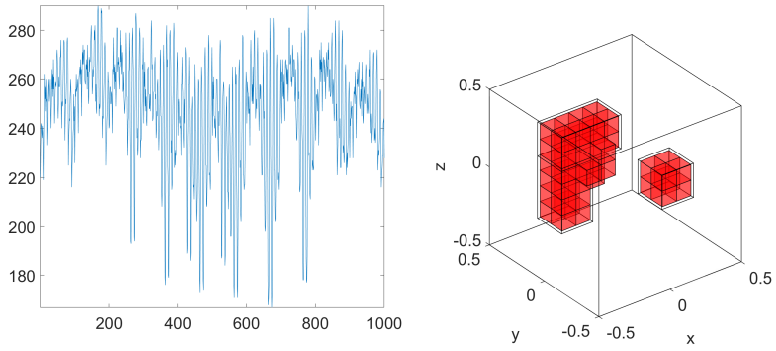

FIG. 5.9. *Left: Plot of the number of negative eigenvalues (y-axis) with block index on the x-axis. Right: Shape reconstruction in 3D space for* $\omega = 50\,rad/s$ *(*$l_p = 1.79\,m$*,* $l_s = 0.18\,m$ *for the homogeneous background material) without noise* $\eta = 0$ *and* $\tilde{M}_l = 198$*.*

ETNA
Kent State University and
Johann Radon Institute (RICAM)

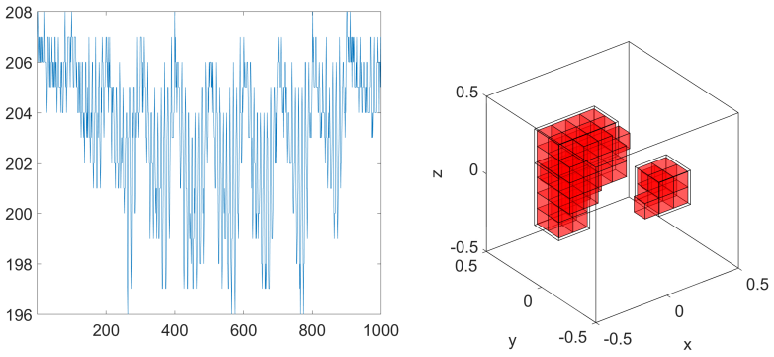

FIG. 5.10. *Left: Plot of the number of negative eigenvalues (y-axis) with block index on the x-axis. Right: Shape reconstruction in 3D space for* $\omega = 50\,rad/s$ *(*$l_p = 1.79\,m$*,* $l_s = 0.18\,m$ *for the homogeneous background material) for noise level* $\eta = 0.003$*,* $\delta = 6.55 \cdot 10^{-6}$*, and* $\tilde{M}_l = 198$*.*

6. Conclusion and outlook. We showed that the standard as well as linearized monotonicity methods for the time-harmonic wave equation can handle noisy data. This is important for simulations based on real-world data, e.g., laboratory data. Here, we remark again that our monotonicity methods work for stochastic as well as deterministic errors and can be applied to problems with all kinds of noise, e.g., noise from measurement or model errors. As a future step we will apply our monotonicity methods to laboratory data. Furthermore, we aim to extend our methods via a monotonicity-based regularization similarly to [12].

Acknowledgments. The author thanks the German Research Foundation (DFG) for funding the project "Inclusion Reconstruction with Monotonicity-based Methods for the Elasto-oscillatory Wave Equation" (reference number 499303971) at the Goethe-University Frankfurt, where the major part of this article has been conducted during this project.

REFERENCES

[1] H. AMMARI, E. BRETIN, J. GARNIER, H. KANG, H. LEE, AND A. WAHAB, *Mathematical Methods in Elasticity Imaging*, Princeton University Press, Princeton, 2015.
[2] W. AQUINO AND M. BONNET, *Analysis of the error in constitutive equation approach for time-harmonic elasticity imaging*, SIAM J. Appl. Math., 79 (2019), pp. 822–849.
[3] G. BAL, C. BELLIS, S. IMPERIALE, AND F. MONARD, *Reconstruction of constitutive parameters in isotropic linear elasticity from noisy full-field measurements*, Inverse Problems, 30 (2014), Paper No. 125004, 22 pages.
[4] G. BAO, T. YIN, AND F. ZENG, *Multifrequency iterative methods for the inverse medium scattering problems in elasticity*, SIAM J. Sci. Comput., 41 (2019), pp. B721–B745.
[5] P. E. BARBONE AND N. H. GOKHALE, *Elastic modulus imaging: on the uniqueness and nonuniqueness of the elastography inverse problem in two dimensions*, Inverse Problems, 20 (2004), pp. 283–296.
[6] J. A. BARCELÓ, M. FOLCH-GABAYET, S. PÉREZ-ESTEVA, A. RUIZ, AND M. C. VILELA, *Uniqueness for inverse elastic medium problems*, SIAM J. Math. Anal., 50 (2018), pp. 3939–3962.
[7] M. BAUMANN, *Fast Iterative Solution of the Time-harmonic Elastic Wave Equation at Multiple Frequencies*, PhD. Thesis, Delft University of Technology, Delft, 2018.
[8] E. BERETTA, M. V. DE HOOP, E. FRANCINI, S. VESSELLA, AND J. ZHAI, *Uniqueness and Lipschitz stability of an inverse boundary value problem for time-harmonic elastic waves*, Inverse Problems, 33 (2017), Paper No. 035013, 27 pages.
[9] E. BERETTA, M. V. DE HOOP, AND L. QIU, *Lipschitz stability of an inverse boundary value problem for time-harmonic elastic waves, part I: recovery of the density*, in Proceedings of the Project Review, Geo-Mathematical Imaging Group, Vol. 1, Purdue University, West Lafayette, 2013, pp. 263–272.

ETNA
Kent State University and
Johann Radon Institute (RICAM)

[10] A. CHARALAMBOPOULOS, A. KIRSCH, K. A. ANAGNOSTOPOULOS, D. GINTIDES, AND K. KIRIAKI, *The factorization method in inverse elastic scattering from penetrable bodies*, Inverse Problems, 23 (2007), pp. 27–51.

[11] S. EBERLE AND B. HARRACH, *Shape reconstruction in linear elasticity: standard and linearized monotonicity method*, Inverse Problems, 37 (2021), Paper No. 045006, 27 pages.

[12] ———, *Monotonicity-based regularization for shape reconstruction in linear elasticity*, Comput. Mech., 69 (2022), pp. 1069–1086.

[13] S. EBERLE, B. HARRACH, H. MEFTAHI, AND T. REZGUI, *Lipschitz stability estimate and reconstruction of Lamé parameters in linear elasticity*, Inverse Probl. Sci. Eng., 29 (2021), pp. 396–417.

[14] S. EBERLE AND J. MOLL, *Experimental detection and shape reconstruction of inclusions in elastic bodies via a monotonicity method*, Internat. J. Solids Structures, 233 (2021), Paper No. 111169, 11 pages.

[15] S. EBERLE-BLICK AND B. HARRACH, *Resolution guarantees for the reconstruction of inclusions in linear elasticity based on monotonicity methods*, Inverse Problems, 39 (2023), Paper No. 075006, 17 pages.

[16] S. EBERLE-BLICK AND N. HYVÖNEN, *Bayesian experimental design for linear elasticity*, Inverse Probl. Imaging, 18 (2024), pp. 1294–1319.

[17] S. EBERLE-BLICK AND V. POHJOLA, *The monotonicity method for inclusion detection and the time harmonic elastic wave equation*, Inverse Problems, 40 (2024), Paper No. 045018, 43 pages.

[18] ———, *The Linearized Monotonicity Method for Elastic Waves and the Separation of Material Parameters*, SIAM J. Math. Anal., 58 (2026), pp. 2031–2066.

[19] J. ELSCHNER AND G. HU, *Uniqueness and factorization method for inverse elastic scattering with a single incoming wave*, Inverse Problems, 35 (2019), Paper No. 094002, 18 pages.

[20] F. FAUCHER, J. SHI, M. V. DE HOOP, AND H. CALANDRA, *Multi-level elastic full waveform inversion in isotropic media via quantitative Lipschitz stability estimates*, in Proceedings of the Project Review, Geo-Mathematical Imaging Group, Vol. 1, Purdue University, West Lafayette, 2014, pp. 1–34.

[21] P. HÄHNER, *A uniqueness theorem for a transmission problem in inverse electromagnetic scattering*, Inverse Problems, 9 (1993), pp. 667–678.

[22] B. HARRACH AND M. N. MINH, *Enhancing residual-based techniques with shape reconstruction features in electrical impedance tomography*, Inverse Problems, 32 (2016), Paper No. 125002, 21 pages.

[23] B. HARRACH, V. POHJOLA, AND M. SALO, *Dimension bounds in monotonicity methods for the Helmholtz equation*, SIAM J. Math. Anal., 51 (2019), pp. 2995–3019.

[24] ———, *Monotonicity and local uniqueness for the Helmholtz equation in a bounded domain*, Analysis & PDE, 12 (2019), pp. 1741–1771.

[25] B. HARRACH AND M. ULLRICH, *Monotonicity-based shape reconstruction in electrical impedance tomography*, SIAM J. Math. Anal., 45 (2013), pp. 3382–3403.

[26] G. HU, A. KIRSCH, AND M. SINI, *Some inverse problems arising from elastic scattering by rigid obstacles*, Inverse Problems, 29 (2013), Paper No. 015009, 21 pages.

[27] G. HU, Y. LU, AND B. ZHANG, *The factorization method for inverse elastic scattering from periodic structures*, Inverse Problems, 29 (2013), Paper No. 115005, 25 pages.

[28] G. HU, A. MANTILE, M. SINI, AND T. YIN, *Direct and inverse time-harmonic elastic scattering from point-like and extended obstacles*, Inverse Probl. Imaging, 14 (2020), pp. 1025–1056.

[29] L. JI, R. MCLAUGHLIN, D. RENZI, AND J.-R. YOON, *Interior elastodynamics inverse problems: shear wave speed reconstruction in transient elastography*, Inverse Problems, 19 (2003), pp. S1–S29.

[30] X. JI AND X. LIU, *Inverse elastic scattering problems with phaseless far field data*, Inverse Problems, 35 (2019), Paper No. 114004, 39 pages.

[31] P. LI, Y. WANG, Z. WANG, AND Y. ZHAO, *Inverse obstacle scattering for elastic waves*, Inverse Problems, 32 (2016), Paper No. 115018, 24 pages.

[32] J. LIU, X. LIU, AND J. SUN, *Extended sampling method for inverse elastic scattering problems using one incident wave*, SIAM J. Imaging Sci., 12 (2019), pp. 874–892.

[33] A. TAMBURRINO, *Monotonicity based imaging methods for elliptic and parabolic inverse problems*, J. Inverse Ill-Posed Probl., 14 (2006), pp. 633–642.

[34] A. TAMBURRINO AND G. RUBINACCI, *A new non-iterative inversion method for electrical resistance tomography*, Inverse Problems, 18 (2002), pp. 1809–1829.

[35] A. B. WEGLEIN, F. V. ARAÚJO, P. M. CARVALHO, R. H. STOLT, K. H. MATSON, R. T. COATES, D. CORRIGAN, D. J. FOSTER, S. A. SHAW, AND H. ZHANG, *Inverse scattering series and seismic exploration*, Inverse Problems, 19 (2003), pp. R27–R83.